THE ASTROPHYSICAL JOURNAL, 494:567–580, 1998 February 20

ULTRAVIOLET SPECTROSCOPY OF THE QUASAR PAIR LB 9605, LB 9612 WITH THE *HUBBLE SPACE TELESCOPE*: EVOLUTION IN THE SIZE OF THE Lyα ABSORBERS?[1]

NADINE DINSHAW,[2,3] CRAIG B. FOLTZ,[4] CHRIS D. IMPEY,[2] AND RAY J. WEYMANN[5]
Received 1996 March 4; accepted 1997 September 24

ABSTRACT

Ultraviolet spectroscopy has been obtained with the faint object spectrograph of the *Hubble Space Telescope* in the Lyα forest of the quasar pair, LB 9605 ($z_{em} = 1.834$) and LB 9612 ($z_{em} = 1.898$), in order to measure the size of the Lyα absorbers. The quasars are separated by 1.′65 on the sky corresponding to a proper separation of 412 h^{-1} kpc at $z = 1.83$ (where $h \equiv H_0/100$ km s^{-1} Mpc^{-1}; $q_0 = 0.5$). We detect five Lyα absorption lines common to both spectra within a velocity difference of 400 km s^{-1} in the redshift range $1.06 < z < 1.69$, and 20 lines which are seen in the spectrum of one quasar but not the other. The number of coincidences expected for randomly distributed absorbers in this redshift interval is 3.2 ± 1.8, implying a less than 2 σ significance for the observed coincidences. If none of the observed coincidences are real, then we can place an upper limit on the absorber radius with 95% confidence of ~ 285 h^{-1} kpc for redshifts $1.06 < z < 1.69$. If, on the other hand, all of the observed coincidences are real, then a maximum likelihood estimate of the characteristic absorber radius in the context of identical, spherical clouds give a most probable radius of 380 h^{-1} kpc with 95% confidence that the characteristic radius lies in the range $305 < R < 595$ h^{-1} kpc. Taken together with a low redshift estimate and new ground-based estimates, the upper limit on the absorber size provides tantalizing evidence for evolution in the radius of the Lyα absorbers with cosmic time, in the sense that the characteristic size of the Lyα absorbers increases with decreasing redshift.

Subject headings: intergalactic medium — quasars: absorption lines — quasars: individual (LB 9605, LB 9612) — ultraviolet: galaxies

1. INTRODUCTION

The Lyα forest absorption lines, observed in the spectra of all quasars at wavelengths shortward of the emission redshift of the quasar, have important implications for cosmology since they may be used to trace the formation and evolution of structure from $z \simeq 5$ to the present (Cen et al. 1994). Recent studies of the Lyα absorbers have changed our perception of their origin and physical characteristics considerably. At low redshifts, Lanzetta et al. (1995) have found that 35% and perhaps as many as 65% of intermediate column-density [$\log N$ (H I) $\gtrsim 14$] Lyα absorption systems arise in the extended envelopes of bright galaxies, whereas low column-density absorbers have been found in or near voids in the galaxy distribution (Morris et al. 1993; Stocke et al. 1995). Very high-resolution observations taken with the Keck telescope imply significant metal enrichment of the absorbers (Tytler et a. 1995; Cowie et al. 1995), and there is growing evidence that the high-column density absorbers are clustered on small scales, although not as strongly as luminous galaxies (Chernomordik 1995; Christiani et al. 1995). Spectroscopic observations of a quasar pair with the *Hubble Space Telescope* (*HST*) have led to a picture of absorbing clouds at $z \simeq 0.5$ that are larger in extent than previously thought and surprisingly quiescent (Dinshaw et al. 1995, hereafter D95). Finally, recent N-body + hydrodynamic simulations produce, as a natural extention of a hierarchical clustering, Lyα forest structures in the form of sheets and filaments with coherence lengths as great as 1 Mpc (Cen et al. 1994; Zhang, Anninos, & Norman 1995; Hernquist et al. 1996; Miralda-Escudé et al. 1996).

Lines of sight to quasar pairs provide a powerful means of diagnosing absorber size and kinematics as derived from the number of Lyα systems observed to be in common between the two lines of sight (LOSs) and the velocity difference between the common systems. In this paper, we use the quasar pair, LB 9605 and LB 9612, to set limits on the size of the Lyα absorption clouds in the critical redshift interval $1.06 < z < 1.69$, lying between a low-redshift *HST* measurement (D95) and two recent ground-based estimates (Dinshaw et al. 1994, hereafter D94; Bechtold et al. 1994). This pair belongs to a group of four quasars projected within 2.°8 on the sky. LB 9605 and LB 9612 have emission redshifts $z_{em} = 1.834$ and 1.898, respectively, and are separated by 1.′65, corresponding to a proper separation of 412 h^{-1} kpc at $z = 1.83$. Spectra of all four quasars in the group were recently analyzed by Elowitz, Green & Impey (1995; hereafter E95) for clustering of the Lyα absorbers on scales ranging from 400 h^{-1} kpc out to 30 h^{-1} Mpc. No evidence was found for a correlation of the Lyα absorbers on the scales of clusters or superclusters, implying the absorbers are smaller in extent than those structures. The LB pair is particularly important for further study since there are currently no meaningful upper limits on the size of the Lyα absorbers.

The observations and reductions are described in § 2, and the method used to select and identify the absorption lines

[1] Based on observation with the NASA/ESA *Hubble Space Telescope*, obtained at the Space Telescope Science Institute, which is operated by the Association of Universities for Research in Astronomy, Inc., under NASA contract NAS5-26555.

[2] Steward Observatory, University of Arizona, Tucson, AZ 85721.

[3] Present Address: UCO/Lick Observatory, University of California, Santa Cruz, CA 95064.

[4] Multiple Mirror Telescope Observatory, University of Arizona, Tucson, AZ 85721.

[5] Carnegie Observatories, 813 Santa Barbara Street, Pasadena, CA 91101-1292.

TABLE 1

PROGRAM QUASARS

QSO	R.A. (J2000)	Decl. (J2000)	V	z_{em}
LB 9605.....	15 19 13.4	23 46 57.4	18.4	1.834
LB 9612.....	15 19 19.4	23 46 03.3	16.4	1.898

NOTE.—Units of right ascension are hours, minutes, and seconds, and units of declination are degrees, arcminutes, and arcseconds.

is discussed in § 3. In § 4, we place constraints on the size of the Lyα absorbers, and finally, in § 5 we summarize and discuss our main results. Throughout this paper, we express all dimensions in terms of the dimensionless Hubble constant $h \equiv H_0/(100 \text{ km s}^{-1} \text{ Mpc}^{-1})$ and take $q_0 = 0.5$.

2. OBSERVATIONS AND REDUCTIONS

LB 9605 was observed on 1995 January 25 and LB 9612 on 1994 December 9 with the faint object spectrograph (FOS) on the refurbished *Hubble Space Telescope*. The observations were taken through the 1″ circular aperture with the red Digicon and G270H grating, and covered the wavelength range 2225–3275 Å. The reciprocal dispersion of the G270H grating is 0.5 Å pixel^{-1}, corresponding to a spectral resolution of 2.0 Å (FWHM). The same guide stars were used in order to minimize radial pointing errors arising from relative placements of the quasars in the aperture. A total of 140 minutes integration time was accumulated on LB 9605 and 49 minutes on LB 9612. Table 1 lists the J2000 coordinates, apparent visual magnitudes and emission redshifts of the program quasars. The coordinates were obtained from the Space Telescope Science Institute using its Guide Star Selection Systems Astrometric Support Package (GASP) and should be accurate to about 1″.

The spectra were reduced via the STSDAS pipeline processing facility, using post-COSTAR "superflats" (Lindler et al. 1993) and inverse sensitivity files. In order to minimize the uncertainty in the wavelength calibration due to nonrepeatability in the positioning of the filter-grating wheel, we recalibrated the data using an exposure of a PtCrNe comparison lamp obtained at the same time as one exposure of each target. The filter-grating wheel was not moved between the target and lamp exposures. The rms error in the wavelength calibration is 0.14 Å. A zero-point offset between the spectra was calculated from the numerous Galactic absorption features observed with he G270H grating (described below).

Figures 1 and 2 show the flux-calibrated spectra of LB 9605 and LB 9612, respectively, and the 1 σ uncertainties in the fluxes. The emission lines near 2950 Å in LB 9605 and

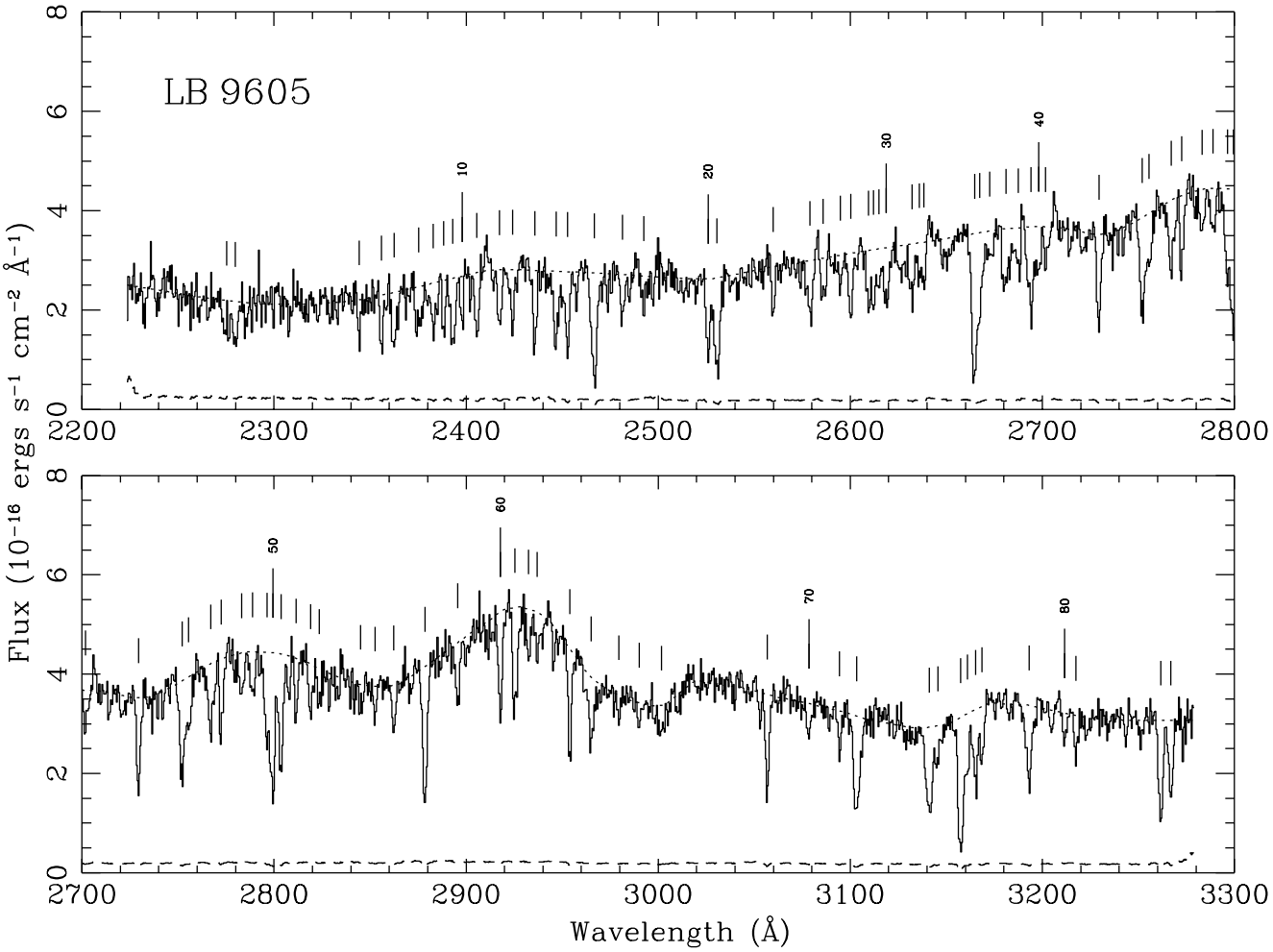

FIG. 1.—*HST* FOS spectrum of LB 9605 as a function of vacuum wavelength. Dashed line in each panel is the 1 σ error in the flux. Dotted line is the continuum fit. Tickmarks indicate absorption features detected at the 3.5 σ or greater confidence level. The emission feature near 2950 Å is Lyβ + O VI $\lambda\lambda$1031, 1037.

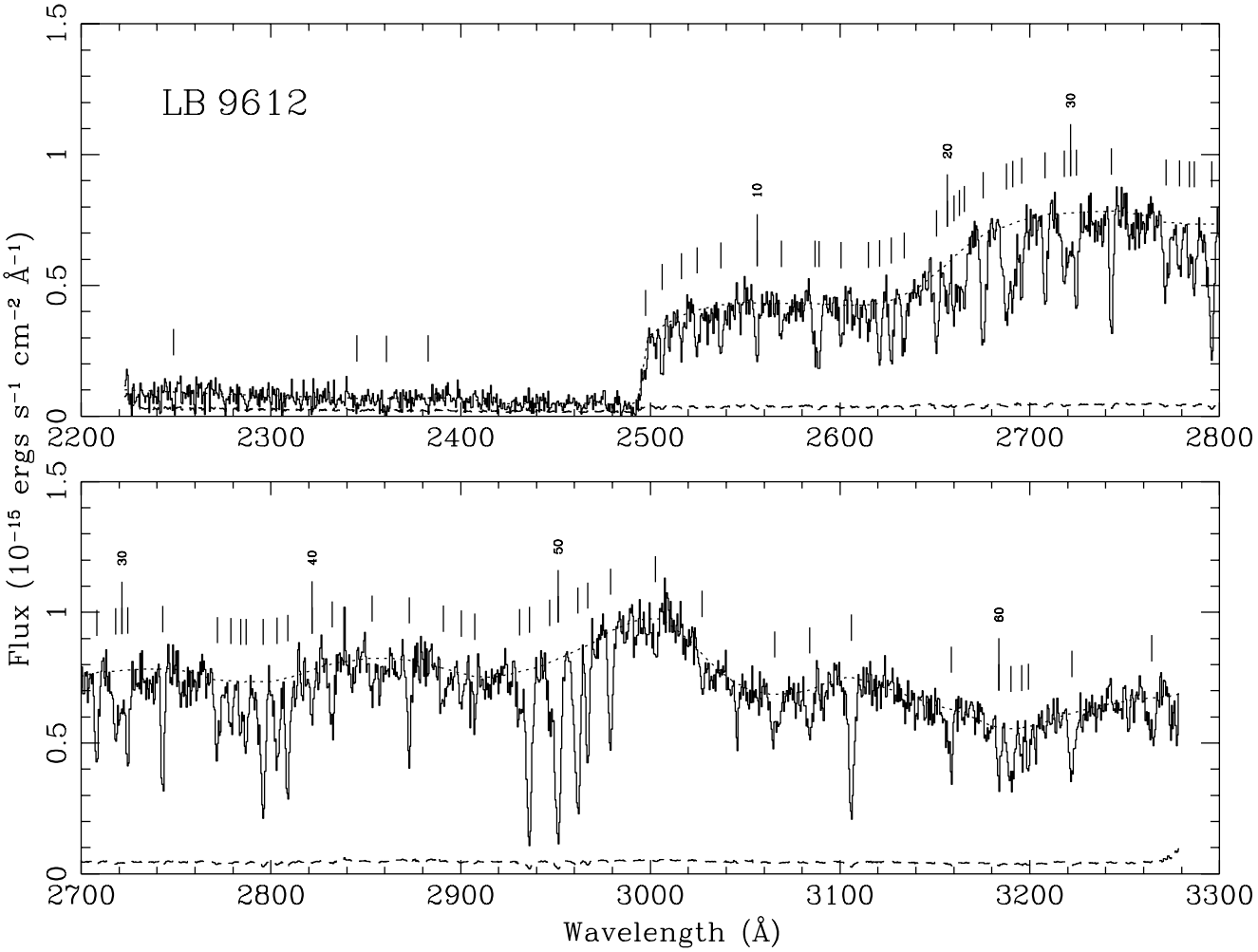

FIG. 2.—Same as Fig. 1 for LB 9612. The emission feature near 3000 Å is Lyβ + O VI $\lambda\lambda$1031, 1037.

3000 Å in LB 9612 are blends of Lyβ + O VI $\lambda\lambda$1031, 1037. The spectrum of LB 9612 exhibits a strong Lyman-limit system (LLS) at $z_{\rm LLS} \simeq 1.7259$ (which we discuss in more detail in § 3). The continuum of each spectrum was determined by fitting cubic splines to binned data points that did not reside insider aborption features. We used the interactive program written by T. Aldcroft (Aldcroft 1993) for this procedure, as well as to select and measure the lines (see § 3). The continua of LB 9605 and LB 9612 are shown as dotted curves in Figures 1 and 2. Because of the difficulty in simultaneously obtaining a good fit over the entire spectrum, some manual adjustments in the continuum were made within heavily blended regions, in the emission line profiles and in the LLS of LB 9612.

Observations of the quasars with the G190H grating were also obtained but are not presented here because the LLS in the spectrum of LB 9612 removes most of the flux below 2500 Å, rendering the data unsuitable for the purpose of this paper.

3. LINE SELECTION AND IDENTIFICATION

A detailed description of the line selection and identification procedures is presented in a separate paper (Dinshaw et al. 1997, hereafter D97); we provide only a brief description here. The spectra were divided by their respective continuum fits, and the normalized spectra searched for significant lines using the method of optimal extraction used for the *HST* Quasar Absorption Line Key Project data and described by Schneider et al. (1993). All the candidate absorption features were then fitted with single, or in the case of obvious blends, multiple Gaussians unconstrained in FWHM, equivalent width and central wavelength. Preliminary lists of the absorption features detected at or above the 3.5 σ confidence level in LB 9605 and LB 9612 are presented in Tables 2 and 3, and the lines in the tables are indicated by tickmarks in Figures 1 and 2, respectively. The quoted confidence levels represent the signal-to-noise ratio (SNR) of the lines defined as SNR = $W/\sigma(W)$, where W is the equivalent width and $\sigma(W)$ the 1 σ uncertainty in the measured W. (This is to be distinguished from the significance level SL used by the Key Project and defined in Schneider et al. 1993). The 3.5 σ line lists were constructed solely for the purpose of identifying the lines and are by no means complete, in the sense that they may include spurious lines or exclude real lines. Only those lines at or above the 5 σ confidence level are considered secure.

The instrumental resolution for the configuration used to obtain the data is listed in the FOS Instrument Handbook (Version 6.0 1995 June) as being 2.0 Å. We found, however, that the widths of about 25% of the lines are smaller than the FWHM of the instrumental line-spread function (LSF). This could arise from a variety of factors, including noise and a continuum fit that is too low across the line.

TABLE 2

THE ABSORPTION LINES OF LB 9605

Number	λ_{obs} (Å)	σ_λ (Å)	W_{obs} (Å)	σ_W (Å)	SNR	FWHM (Å)	ID	z_{abs}	Remarks
1	2275.27	0.42	1.32	0.30	4.5	4.13	Lyα	0.8716	
2	2279.95	0.25	1.12	0.25	4.4	2.59	Lyα	0.8755	
3	2344.46	0.10	0.72	0.10	6.9	2.00	Fe II 2344	0.0001	
4	2356.01	0.10	0.89	0.12	7.8	1.61	Lyα	0.9380	
5	2362.61	0.15	1.47	0.15	9.8	3.02	Lyα	0.9435	
6	2375.35	0.22	1.39	0.17	8.2	3.75	Fe II 2374	0.0004	
7	2383.08	0.21	1.37	0.16	8.5	3.68	Fe II 2382	0.0001	
8	2388.41	0.11	0.80	0.11	7.5	1.67	Lyα	0.9647	
9	2393.13	0.11	1.63	0.13	12.5	2.94	Lyϵ	1.5518	[a]
10	2397.94	0.13	0.73	0.11	6.9	1.87	Lyθ	1.5976	
11	2405.58	0.10	1.15	0.11	10.5	2.30	Lyη	1.5972	
12	2417.43	0.12	1.06	0.11	9.3	2.38	Lyα	0.9886	
13	2424.10	0.13	0.97	0.11	8.8	2.27	Lyδ	1.5524	
14	2435.76	0.09	1.25	0.12	10.4	1.97	Lyϵ	1.5973	
15	2446.85	0.13	1.94	0.15	13.2	3.57	Lyα	1.0128	
16	2452.77	0.08	1.61	0.11	14.2	2.56	Lyα	1.0176	
17	2466.79	0.06	2.87	0.11	25.0	3.41	Lyδ	1.5973	[b]
18	2481.34	0.14	0.79	0.10	7.6	2.21	Lyγ	1.5514	
19	2492.46	0.21	0.57	0.13	4.6	1.99	Lyβ	1.4300	
20	2526.01	0.07	1.48	0.11	13.9	2.28	Lyγ	1.5973	
21	2530.66	0.07	2.66	0.12	21.5	3.48	Lyα	1.0817	
22	2559.90	0.10	0.66	0.08	8.0	1.66	Lyα	1.1058	[c]
23	2579.10	0.14	1.31	0.11	11.5	3.25	Lyβ	1.5144	
24	2586.06	0.14	0.66	0.09	7.3	2.11	Fe II 2586	−0.0002	
25	2594.79	0.21	0.52	0.10	5.5	2.33	Lyα	1.1345	[d]
26	2600.21	0.09	1.06	0.09	11.9	2.32	Fe II 2600	0.0000	
	2600.21	0.09	1.06	0.09	11.9	2.32	Lyη	1.8064	[e]
27	2609.53	0.12	0.84	0.11	7.8	2.05	Lyγ	1.6832	
28	2612.06	0.21	0.74	0.10	7.5	1.95	Lyζ	1.8064	[e]
29	2614.96	0.28	0.71	0.17	4.1	2.91	Lyα	1.1510	
30	2618.86	0.14	1.19	0.12	10.2	3.19	Lyβ	1.5532	
31	2632.13	0.15	1.15	0.11	10.3	3.26	Lyϵ	1.8067	[e]
32	2635.80	0.21	0.51	0.13	4.0	2.26	Lyγ	1.7102	[f]
33	2638.37	0.15	0.57	0.10	5.9	1.95	Lyα	1.1703	
34	2664.37	0.16	2.41	0.36	6.7	2.70	Lyβ	1.5976	
	2664.37	0.16	2.41	0.36	6.7	2.70	Lyδ	1.8054	[e]
35	2667.18	0.20	1.31	0.24	5.5	2.61	Lyβ	1.6003	[g]
36	2672.86	0.39	0.54	0.14	3.9	3.34	Lyγ	1.7483	[h,i]
37	2681.16	0.18	1.61	0.13	12.7	4.87	Lyα	1.2055	
38	2687.44	0.19	0.68	0.10	6.7	2.69	Lyα	1.2107	
39	2693.99	0.14	1.85	0.16	11.5	3.68	Lyβ	1.6264	
40	2698.18	0.22	0.73	0.15	4.8	2.69	Lyα	1.2195	
41	2701.91	0.18	0.62	0.09	7.1	2.59	Lyδ	1.8449	[j]
42	2729.43	0.06	1.27	0.07	17.7	2.16	Lyγ	1.8065	[e]
43	2752.08	0.12	1.51	0.16	9.3	2.72	Lyβ	1.6831	[k]
44	2755.63	0.27	0.88	0.17	5.2	3.14	Lyβ	1.6865	[l]
45	2767.14	0.13	1.15	0.09	12.7	3.42	Lyγ	1.8453	[j]
46	2772.47	0.08	0.79	0.07	12.0	1.92	Lyβ	1.7029	[m]
47	2782.95	0.29	0.70	0.10	6.7	4.01	Lyβ	1.7132	[f]
48	2788.92	0.20	0.59	0.09	6.8	2.84	Lyβ	1.7190	[n]
49	2796.36	0.26	0.84	0.06	13.1	2.03	Mg II 2796	0.0000	
50	2799.23	0.06	2.22	0.11	20.6	3.12	Lyβ	1.7290	[o]
51	2803.65	0.06	1.50	0.08	18.6	2.50	Mg II 2803	0.0000	
	2803.65	0.06	1.50	0.08	18.6	2.50	Lyβ	1.7333	[p]
52	2811.51	0.10	0.52	0.06	8.3	1.63	Lyβ	1.7410	[q]
53	2819.07	0.13	0.58	0.07	7.9	2.16	Lyβ	1.7484	[h]
54	2823.55	0.21	0.44	0.08	5.5	2.33	Lyβ	1.7527	[r]
55	2845.18	0.27	0.34	0.09	3.9	2.21	Lyβ	1.7738	[s]
56	2852.58	0.22	0.34	0.06	5.5	2.00	Mg I 2853	−0.0001	
57	2862.39	0.14	0.52	0.07	7.1	1.97	Lyβ	1.7906	[t]
58	2878.56	0.05	1.85	0.07	25.7	2.62	Lyβ	1.8064	[e]
59	2895.67	0.12	0.70	0.07	9.5	2.42	Lyβ	1.8231	[u]
60	2917.89	0.07	0.98	0.06	15.6	2.23	Lyβ	1.8447	[j]
61	2925.43	0.08	1.23	0.07	17.3	2.90	Lyα	1.4064	
62	2932.63	0.16	0.44	0.07	6.6	2.21	Lyα	1.4124	[d]
63	2937.05	0.18	0.45	0.07	6.3	2.34	Lyα	1.4160	[d]
64	2954.03	0.05	1.13	0.06	18.1	2.01	Lyα	1.4300	
65	2965.15	0.13	0.98	0.12	8.0	2.65	Lyα	1.4391	
66	2979.51	0.21	0.27	0.07	3.8	1.60	Lyα	1.4509	[d]
67	2990.06	0.20	0.28	0.07	3.9	1.62	Lyα	1.4596	[d]
68	3001.71	0.42	0.88	0.14	6.3	5.60	Lyα	1.4692	
69	3056.80	0.05	1.33	0.07	18.7	2.16	Lyα	1.5145	

TABLE 2—*Continued*

Number	λ_{obs} (Å)	σ_λ (Å)	W_{obs} (Å)	σ_W (Å)	SNR	FWHM (Å)	ID	z_{abs}	Remarks
70	3078.44	0.19	0.49	0.09	5.7	2.29	Lyα	1.5323	
71	3094.48	0.11	0.51	0.07	7.2	1.63	Lyα	1.5455	
72	3103.38	0.07	2.52	0.10	24.9	3.88	Lyα	1.5528	
73	3141.14	0.11	2.52	0.16	15.5	3.97	Lyα	1.5839	
74	3145.52	0.28	0.65	0.15	4.2	2.83	Lyα	1.5875	
75	3157.56	0.06	3.13	0.14	23.1	3.32	Lyα	1.5974	
76	3161.10	0.14	0.83	0.14	5.8	2.28	Lyα	1.6003	
77	3165.15	0.12	1.08	0.13	8.6	2.30	Lyα	1.6036	
78	3168.41	0.18	0.93	0.14	6.7	2.69	Lyα	1.6063	
79	3193.10	0.10	1.68	0.10	17.4	3.46	Lyα	1.6267	
80	3211.63	0.22	0.38	0.09	4.3	1.92	Lyα	1.6419	
81	3217.55	0.15	0.58	0.09	6.5	1.99	Lyα	1.6467	
82	3261.73	0.06	1.86	0.09	20.9	2.57	Lyα	1.6831	[v]
83	3266.95	0.09	1.33	0.10	13.1	2.50	Lyα	1.6874	[v]

[a] Lyϵ is too strong with respect to other lines in this system and is almost certainly a blend.
[b] Possibly blended with Lyβ of system $z = 1.4064$.
[c] System may contain absorption from heavy elements (see footnote v).
[d] Possibly spurious.
[e] Corresponding Lyα identified as system $z = 1.8078$ in E95.
[f] Corresponding Lyα identified as system $z = 1.7183$ in E95.
[g] Possibly blended with Lyγ of system $z = 1.7410$.
[h] Corresponding Lyα identified as system $z = 1.7522$ in E95.
[i] Possibly blended with Lyβ of systems $z = 1.6036$ and 1.6063.
[j] Corresponding Lyα identified as system $z = 1.8465$ in E95.
[k] Corresponding Lyα identified as system $z = 1.6908$ in E95.
[l] Corresponding Lyα identified as system $z = 1.6956$ in E95.
[m] Corresponding Lyα identified as system $z = 1.7097$ in E95.
[n] Corresponding Lyα identified as system $z = 1.7245$ in E95.
[o] Corresponding Lyα identified as system $z = 1.7334$ in E95. Lyβ is stronger than Lyα and is possibly a blend.
[p] Corresponding Lyα identified as system $z = 1.7366$ in E95.
[q] Corresponding Lyα identified as system $z = 1.7447$ in E95.
[r] Corresponding Lyα identified as system $z = 1.7567$ in E95.
[s] Corresponding Lyα identified as system $z = 1.7768$ in E95.
[t] Corresponding Lyα identified as system $z = 1.7942$ in E95.
[u] Corresponding Lyα identified as system $z = 1.8241$ in E95.
[v] Uncertain identification. Possibly C IV λλ1548, 1550 at $z = 1.1068$. C II λ1334 would be blended with Lyβ of system $z = 1.7411$. Lyα at $z = 1.1058$ is possibly associated with the C IV doublet.

The approach of the Key Project under these circumstances is to fit the narrow lines again with the FWHM fixed at the instrumental LSF. A consequence of this approach to our analysis (where we have defined the significance of a line by its SNR) is that the SNRs of many of the weaker lines would be overestimated, some by as much as 50%, because the uncertainty in the measurement of the equivalent is artificially smaller having removed one degree of freedom in the fit. In order to find a more acceptable solution, we plotted a histogram of the FWHMs of all the lines. The histogram showed a smooth distribution of FWHMs with a peak at 2.2 Å and a sharp break in the number of lines with FWHMs less than 1.6 Å. Assuming that many of the lines with FWHM < 1.6 Å are likely spurious, we included in Tables 2 and 3 only those lines with FWHM ≥ 1.6 Å. This excluded eight lines from the line list of LB 9605 and six lines from that of LB 9612. By allowing the FWHM to vary during the line fitting, we have ensured that we have not overestimated the significance of a line with FWHM < 2.0 Å, such that it could spuriously appear in our 5 σ line list (defined below), but we note that the equivalent widths of those lines are likely underestimated.

The identification of the lines was problematic due to the limited spectral range and significant level of crowding in our data. To minimize the uncertainty in the line identifications, we extended the wavelength coverage of the data out to the Lyα emission using spectra published by E95. However, because of problems with the wavelength calibration of the ground-based data, some of the identifications remain insecure, as indicated in the footnotes in Tables 2 and 3. We have followed closely the approach implemented in the Key Project program ZSEARCH (Bahcall et al. 1996) for identifying the lines with two exceptions: we carried out the identifications manually, and we used a subset of 53 strong ultraviolet absorption lines from Morton, York, & Jenkins (1988). We first searched the spectra for plausible Galactic interstellar lines. Then, we looked for Lyβ lines that corresponded to the Lyα systems identified by E95 before searching for new systems. Starting from the red ends of the FOS spectra, we treated each significant absorption line as a candidate Lyα line and searched for higher order Lyman series lies corresponding to that system. Once we identified a system, we checked that relative equivalent widths of the lines in that system were consistent with their known oscillator strengths. Finally, the spectra were scanned for doublets of C IV λλ1548, 1550, Si IV λλ1393, 1402, N V λλ1238, 1242, and O VI λλ1031, 1037, and features associated with those systems. We found 15 Lyα absorption systems in both LB 9605 and LB 9612 with $W_0 > 0.32$ Å, consistent with the expected number ($\sim 16 \pm 4$) given the number density of Lyα lines per unit redshift determined from the Quasar Absorption Line Key Project (Bahcall et al. 1993), which lends some confidence to our line identifications.

We identified a strong LLS in the spectrum of LB 9612. From the Lyman series lines Lyβ through Lyη associated

with this system, we derive a redshift of $z_{\rm LLS} = 1.7259 \pm 0.0001$ for the LLS. The optical depth of the LLS was estimated from the ratio of the fluxes shortward F_- and longward F_+ of the LLS:

$$\exp(-\tau_{\rm LLS}) \equiv \frac{F_-}{F_+}.$$

F_+ was estimated by fitting the continuum between 2550 and 2600 Å assuming constant flux, and F_- was determined in the wavelength region from 2350 to 2500 Å. Dividing the flux in the continuum from the flux estimated in the LLS, we obtain an optical depth of $\tau_{\rm LLS} = 2.00 \pm 0.07$. This corresponds to an H I column density of $\log N$ (H I) $= 17.50 \pm 0.02$. The uncertainty was estimated by varying the locations and widths of the fitting windows. Another weaker LLS appears to be present in the spectrum of LB 9612 at $z_{\rm LLS} = 1.8879 \pm 0.0001$.

To avoid introducing spurious absorption lines into the analysis, we considered for further study only those Lyα absorption lines detected at or above 5 σ confidence level. Because the S/N degrades rapidly shortward of dthe LLS, we also restricted our sample to lines with wavelengths greater than 2500 Å. In this way, we can be sure that in the range 2500–3270 all lines with $W_0 > 0.32$ Å are detected with 5 σ confidence in *both* objects. Figure 3 shows the observed equivalent width thresholds (5 σ) for unresolved lines as functions of wavelength for LB 9605 (*solid line*) and LB 9612 (*dashed line*). The Lyα lines meeting both criteria are listed in Table 4. We point out that, in order to facilitate future comparison, the selection criteria used in this paper are the same as those used in D95 for the quasar pair Q0107−025A, B.

In Table 4, we have also culled out all Galactic absorption lines and higher order Lyman series lines. Since absorption line systems containing metal lines may have

TABLE 3

THE ABSORPTION LINES OF LB 9612

Number	$\lambda_{\rm obs}$ (Å)	σ_λ (Å)	$W_{\rm obs}$ (Å)	σ_W (Å)	SNR	FWHM (Å)	ID	$z_{\rm abs}$	Remarks
1	2248.79	0.25	1.65	0.44	3.7	2.06	Lyα	0.8498	a
2	2345.39	0.26	1.55	0.44	3.5	2.02	Fe II 2344	0.0006	a
3	2360.84	0.29	2.90	0.55	5.3	3.26	Lyα	0.9420	a
4	2382.91	0.28	1.44	0.29	4.9	2.00	Fe II 2382	0.0001	a
5	2497.47	0.26	0.79	0.22	3.6	1.92	Lyα	1.0544	a
6	2506.26	0.10	1.20	0.14	8.8	1.90	Lyα	1.0616	
7	2516.39	0.14	0.71	0.12	5.8	1.67	Lyθ	1.7259	b
8	2524.79	0.17	1.08	0.15	7.4	2.54	Lyη	1.7259	b
9	2537.26	0.13	1.18	0.14	8.7	2.45	Lyζ	1.7260	b
10	2556.22	0.10	1.12	0.12	9.6	1.98	Lyϵ	1.7258	b
11	2568.97	0.19	0.76	0.14	5.6	2.27	Lyβ	1.5045	
12	2586.74	0.21	1.04	0.22	4.8	2.25	Fe II 2586	0.0000	
	2586.74	0.21	1.04	0.22	4.8	2.25	Lyβ	1.5219	
13	2588.93	0.12	1.22	0.17	7.2	2.00	Lyδ	1.7259	b
14	2600.63	0.14	0.85	0.12	7.0	2.09	Fe II 2600	0.0002	
	2600.63	0.14	0.85	0.12	7.0	2.09	Lyβ	1.5354	
15	2614.96	0.20	0.57	0.12	4.7	1.99	Lyα	1.1510	
16	2620.82	0.09	1.23	0.11	11.0	2.09	Lyβ	1.5551	
17	2627.06	0.10	1.33	0.12	11.4	2.28	Lyϵ	1.8013	c,d
18	2633.74	0.11	1.22	0.12	10.2	2.41	Lyα	1.1665	e
19	2650.89	0.09	1.42	0.11	12.9	2.44	Lyγ	1.7257	b
20	2656.57	0.16	0.89	0.12	7.6	2.60	Lyα	1.1853	
21	2660.07	0.12	0.90	0.12	7.8	2.06	Lyδ	1.8008	d
	2660.07	0.12	0.90	0.12	7.8	2.06	Lyι	1.8884	f
22	2662.88	0.35	0.62	0.09	6.7	2.00	Lyα	1.1905	
23	2665.54	0.16	0.87	0.13	6.5	2.31	Lyβ	1.5987	
	2665.54	0.16	0.87	0.13	6.5	2.31	Lyθ	1.8874	f
24	2675.51	0.07	2.03	0.10	20.4	3.00	Lyη	1.8886	f,g
25	2687.63	0.29	1.94	0.32	6.0	3.75	Lyζ	1.8876	f,h
26	2691.49	0.32	1.21	0.24	5.0	3.14	Lyβ	1.6240	
27	2695.65	0.14	0.88	0.12	7.5	2.19	Lyα	1.2174	
28	2708.16	0.09	1.13	0.09	12.8	2.35	Lyϵ	1.8878	f
29	2718.35	0.24	1.27	0.18	7.2	3.74	Lyβ	1.6502	i
30	2721.50	0.35	0.36	0.09	4.1	1.98	Lyα	1.2387	
31	2724.54	0.09	1.17	0.10	11.6	2.36	Lyγ	1.8015	d
32	2742.97	0.05	1.35	0.08	17.8	2.02	Lyδ	1.8881	f
33	2771.91	0.14	1.31	0.11	11.8	3.44	Lyβ	1.7024	j
34	2779.01	0.18	0.73	0.10	7.2	2.63	Lyβ	1.7093	k
35	2784.01	0.40	0.53	0.09	6.7	1.77	Lyβ	1.7142	l
36	2786.85	0.13	0.88	0.11	8.1	2.30	Lyβ	1.7170	l
37	2795.97	0.08	1.99	0.14	14.0	2.60	Mg II 2796	−0.0001	
	2795.97	0.08	1.99	0.14	14.0	2.60	Lyβ	1.7259	b
38	2803.34	0.11	1.45	0.11	13.0	3.18	Mg II 2803	−0.0001	
39	2808.80	0.06	1.70	0.09	18.8	2.56	Lyγ	1.8881	f
40	2821.65	0.17	0.60	0.09	6.5	2.27	Lyα	1.3211	m
41	2832.22	0.15	0.96	0.10	9.5	2.89	Lyβ	1.7611	n
42	2853.32	0.27	0.53	0.10	5.2	2.83	Mg I 2853	0.0001	

TABLE 3—*Continued*

Number	λ_{obs} (Å)	σ_λ (Å)	W_{obs} (Å)	σ_W (Å)	SNR	FWHM (Å)	ID	z_{abs}	Remarks
43	2872.94	0.09	1.14	0.09	12.0	2.24	Lyβ	1.8009	[d]
44	2890.85	0.31	0.66	0.13	5.1	3.31	Lyα	1.3780	[m,o]
45	2900.41	0.25	0.41	0.09	4.4	2.28	Lyα	1.3859	[m,o]
46	2907.30	0.18	0.53	0.09	5.8	2.12	Lyα	1.3915	[m,o]
47	2931.07	0.21	0.80	0.12	6.9	3.14	Lyα	1.4111	[m]
48	2936.17	0.04	2.96	0.10	29.9	3.23	Lyα	1.4153	[p]
49	2947.00	0.19	0.79	0.12	6.4	2.69	Lyα	1.4242	[m]
50	2951.34	0.05	3.30	0.12	26.7	3.65	Lyα	1.4277	
51	2961.71	0.05	2.74	0.10	28.8	3.53	Lyβ	1.8874	[f,q]
52	2967.00	0.06	1.17	0.08	15.6	2.09	Lyα	1.4406	[q]
53	2978.99	0.08	1.34	0.08	16.2	2.58	Lyα	1.4505	[r]
54	3002.70	0.28	0.45	0.09	4.9	2.81	Lyα	1.4700	[o]
55	3027.40	0.26	0.43	0.10	4.2	2.38	Lyα	1.4903	[o]
56	3065.72	0.31	1.34	0.16	8.5	5.52	Lyα	1.5218	
57	3083.91	0.22	0.95	0.12	7.9	3.57	Lyα	1.5368	
58	3105.99	0.06	2.57	0.10	25.8	3.43	Lyα	1.5550	
59	3158.49	0.09	0.76	0.10	7.8	1.63	Lyα	1.5981	
60	3183.78	0.12	0.85	0.10	8.7	2.07	Lyα	1.6190	
61	3190.15	0.16	1.58	0.14	11.6	3.81	Lyα	1.6242	
62	3195.78	0.17	0.51	0.10	5.3	1.87	Lyα	1.6288	[o]
63	3199.24	0.13	0.59	0.09	6.4	1.71	Lyα	1.6317	
64	3222.16	0.14	1.44	0.12	12.0	3.41	Lyα	1.6505	i
65	3264.40	0.32	1.05	0.16	6.7	4.34	Lyα	1.6853	[s]

[a] Wavelength is highly uncertain since the line lies in the Lyman limit.
[b] Corresponding Lyα identified as system $z = 1.7300$ in E95. Line is associated with the LLS at $z_{LLS} = 1.7259$.
[c] Lyϵ is too strong with respect to other lines in this system and is almost certainly a blend. Possibly blended with Lyγ of system $z = 1.7024$.
[d] Corresponding Lyα identified as system $z = 1.8028$ in E95.
[e] Possibly blended with Lyγ of system $z = 1.7093$.
[f] Corresponding Lyα identified as system $z = 1.8897$ in E95. Line is associated with probable LLS at $z_{LLS} = 1.8879$.
[g] Lyη is too strong with respect to other lines in this system and is almost certainly a blend.
[h] Possibly blended with Lyβ of system $z = 1.6190$, and with Lyγ of system $z = 1.7611$.
[i] Corresponding Lyα identified as system $z = 1.6610$ in E95.
[j] Corresponding Lyα identified as system $z = 1.7093$ in E95.
[k] Corresponding Lyα identified as system $z = 1.7153$ in E95.
[l] Corresponding Lyα identified as one system at $z = 1.7210$ in E95, but is clearly a blend of two systems at $z = 1.7142$ and 1.7170.
[m] Possibly Lyβ.
[n] Corresponding Lyα identified as system $z = 1.7628$ in E95.
[o] Possibly spurious.
[p] System contains absorption from heavy elements. Corresponding C IV doublet identified at $z = 1.4146$ in E95.
[q] Uncertain identification. Possibly C IV $\lambda\lambda$ 1548, 1550 at $z = 0.9131$. No other lines associated with this system are detected, but Lyα would lie in the Lyman limit.
[r] Possibly Lyβ corresponding to Lyα system at $z = 1.9006$ in E95.
[s] Corresponding Lyα identified as system $z = 1.6921$ in E95.

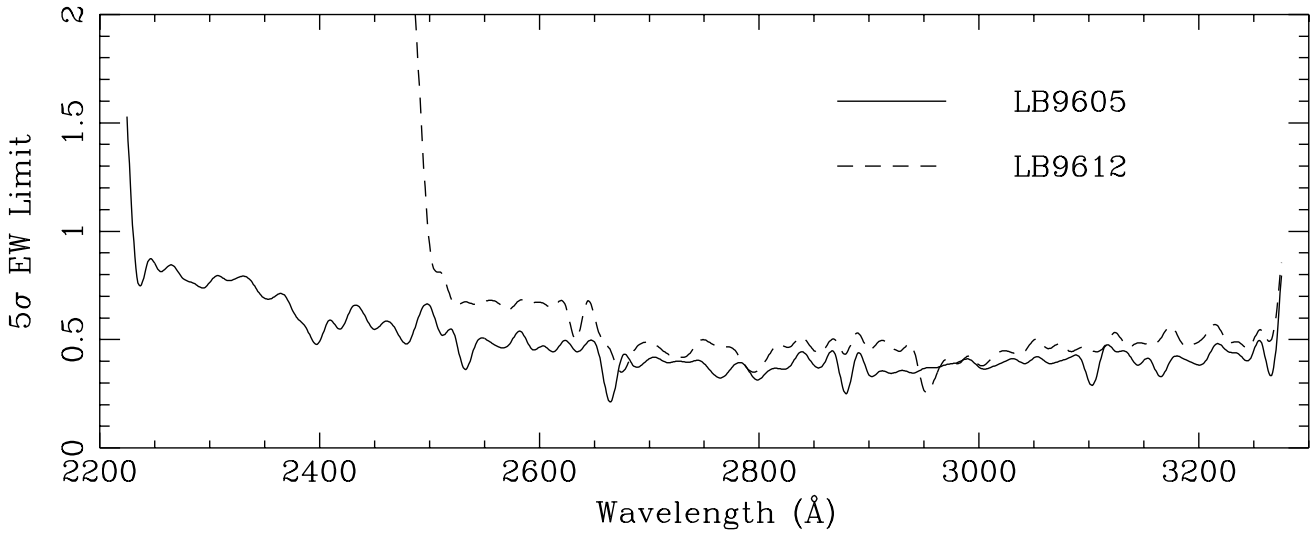

FIG. 3.—Equivalent width thresholds (5 σ) for unresolved lines as functions of wavelength for LB 9605 (*solid line*) and LB 9612 (*dashed line*)

TABLE 4

COINCIDENT AND ANTICOINCIDENT Lyα ABSORPTION SYSTEMS

LB9605							LB9612							
Number	λ (Å)	σ_λ (Å)	W_0 (Å)	σ_W (Å)	SNR	z_{abs}	Number	λ (Å)	σ_λ (Å)	W_0 (Å)	σ_W (Å)	SNR	z_{abs}	LB9605–LB9612 (km s^{-1})
			<0.28				1	2506.04	0.10	0.58	0.07	8.8	1.0614	
1	2530.66	0.07	1.28	0.06	21.5	1.0817				<0.32				
			<0.19				2	2633.51	0.11	0.56	0.06	10.2	1.1663	
			<0.19				3	2656.34	0.16	0.41	0.05	7.6	1.1851	
2	2681.16	0.18	0.73	0.06	12.7	1.2055				<0.22				
			<0.18				4	2695.42	0.14	0.40	0.05	7.5	1.2172	
3	2925.43	0.08	0.51	0.03	17.3	1.4064				<0.19				
			<0.14				5	2930.82	0.21	0.33	0.05	6.9	1.4109	
			<0.14				6	2946.74	0.19	0.33	0.05	6.4	1.4240	
4	2954.03	0.05	0.47	0.02	18.1	1.4300	7	2951.08	0.05	1.36	0.05	26.7	1.4275	300 ± 4
5	2965.15	0.13	0.40	0.05	8.0	1.4391	8	2966.74[a]	0.06	0.48	0.03	15.6	1.4404	-161 ± 7
			<0.16				9	2978.73[b]	0.08	0.55	0.03	16.2	1.4503	
6	3001.71	0.42	0.36	0.06	6.3	1.4692				<0.16				
7	3056.80	0.05	0.53	0.03	18.7	1.5145				<0.19				
			<0.16				10	3065.45	0.31	0.53	0.06	8.5	1.5216	
			<0.16				11	3083.64	0.22	0.37	0.05	7.9	1.5366	
8	3103.38	0.07	0.99	0.04	24.9	1.5528	12	3105.72	0.06	1.01	0.04	25.8	1.5547	-226 ± 4
9	3141.14	0.11	0.98	0.06	15.5	1.5839				<0.19				
10	3157.56	0.06	1.21	0.05	23.1	1.5974				<0.17				
11	3165.15	0.12	0.41	0.05	8.6	1.6036				<0.19				
12	3168.41	0.18	0.36	0.05	6.7	1.6063				<0.20				
13	3193.10	0.10	0.64	0.04	17.4	1.6267	13	3189.87	0.16	0.60	0.05	11.6	1.6240	304 ± 9
			<0.15				14	3221.88	0.14	0.54	0.05	12.0	1.6503	
14	3261.73[c]	0.06	0.69	0.03	20.9	1.6831	15	3264.12	0.32	0.39	0.06	6.7	1.6850	-220 ± 15
15	3266.95[c]	0.09	0.49	0.04	13.1	1.6874				<0.20				

NOTES.—This table lists those lines with rest equivalent widths $W_0 > 0.32$ Å. Upper equivalent width limits are 5 σ confidence level.

[a] Possibly C IV λ1550 with redshift $z_{abs} = 0.9131$. The C IV λ1548 component associated with this possible system has been identified as Lyβ belonging to the certain system at $z_{abs} = 1.8874$ in Table 3.

[b] Possibly Lyβ.

[c] Possibly member of C IV doublet with redshift $z_{abs} = 1.1068$.

different properties than the Lyα-only lines, we selected only those lines that we believe are not members of metal-line containing systems. E95 found no metal-line systems in LB 9605, and one C IV doublet in LB 9612 at $z_{abs} = 1.4146$. Their ground-based data has a 3 σ limiting equivalent width of 0.6–0.7 Å over the observed wavelength range 3200–5500 Å.

There are numerous Galactic absorption features in the wavelength range covered by the G270H grating: Fe II λ2344, λ2374, λ2382, λ2586, λ2600, Mg II $\lambda\lambda$2796, 2803, and Mg I λ2853. Using only the Galactic feature found outside the LLS, we measured the zero-point shift between the spectra of LB 9605 and LB 9612 to be -26 ± 6 km s^{-1}. In Table 4, we have shifted the lines of LB 9612 to the blue by 26 km s^{-1} to register them with the lines of LB 9605.

4. LIMITS ON THE SIZE OF THE Lyα ABSORBERS

The goal of this paper is to put new constraints on the size of Lyα absorbers at the intermediate redshifts $1.06 < z < 1.69$. This is not a trivial task at these redshifts because of the high density of lines, which make the assignment of common systems difficult. In D94 and D95, we defined a Lyα absorption feature to be common, or coincident, if there was a corresponding line in the other spectrum within a velocity difference of ± 150 km s^{-1}. Similarly, we designated a system to be *not* in common, or anticoincident, if there was no corresponding match within the same velocity difference. In all cases, the assignments of coincident and anticoincident systems were unambiguous, in the sense that the histogram of velocity pairs fell in the range ± 150 km s^{-1}, with no more pairs out to several thousand km s^{-1}. On the other hand, the pairwise velocity histogram of the Lyα lines in LB 9605 and LB 9612 shows no clear cutoff velocity (see below). In order to establish the optimum window in which to define coincident and anticoincident pairs, we compare in Figure 4*a* the cumulative velocity difference distribution of the Lyα absorption systems in Table 4, with the distribution expected for randomly-placed absorbers. The velocity differences were computed between each line in LB 9605 and its nearest neighbor in LB 9612, such that every line belonged to one, and only one, pair.

The expected distribution was estimated from 1000 samples of systems (15 per LOS) drawn randomly from the same redshift intervals as the observations. Shortward of 2900 Å, Lyα lines were difficult to detect because of crowding from Lyβ and Galactic absorption lines. Therefore, in calculating the number of random coincidences, we did not draw lines from regions in which Lyα lines were not detected. Roughly, this corresponded to the wavelength regions 2550–2650 Å and 2700–2900 Å in LB 9605, and 2520–2620 Å and 2750–2900 Å in LB 9612.

Figure 4*a* shows that if we restrict the size of the velocity window in which we define a coincidence to be too small, we minimize the number of random coincidences, N_r, but we may also exclude some real coincidences. For example, for $\Delta v = 150$ km s^{-1}, which corresponds to the velocity separations in which common systems were observed in other quasar pairs (see D94 and D95), we find no coincident

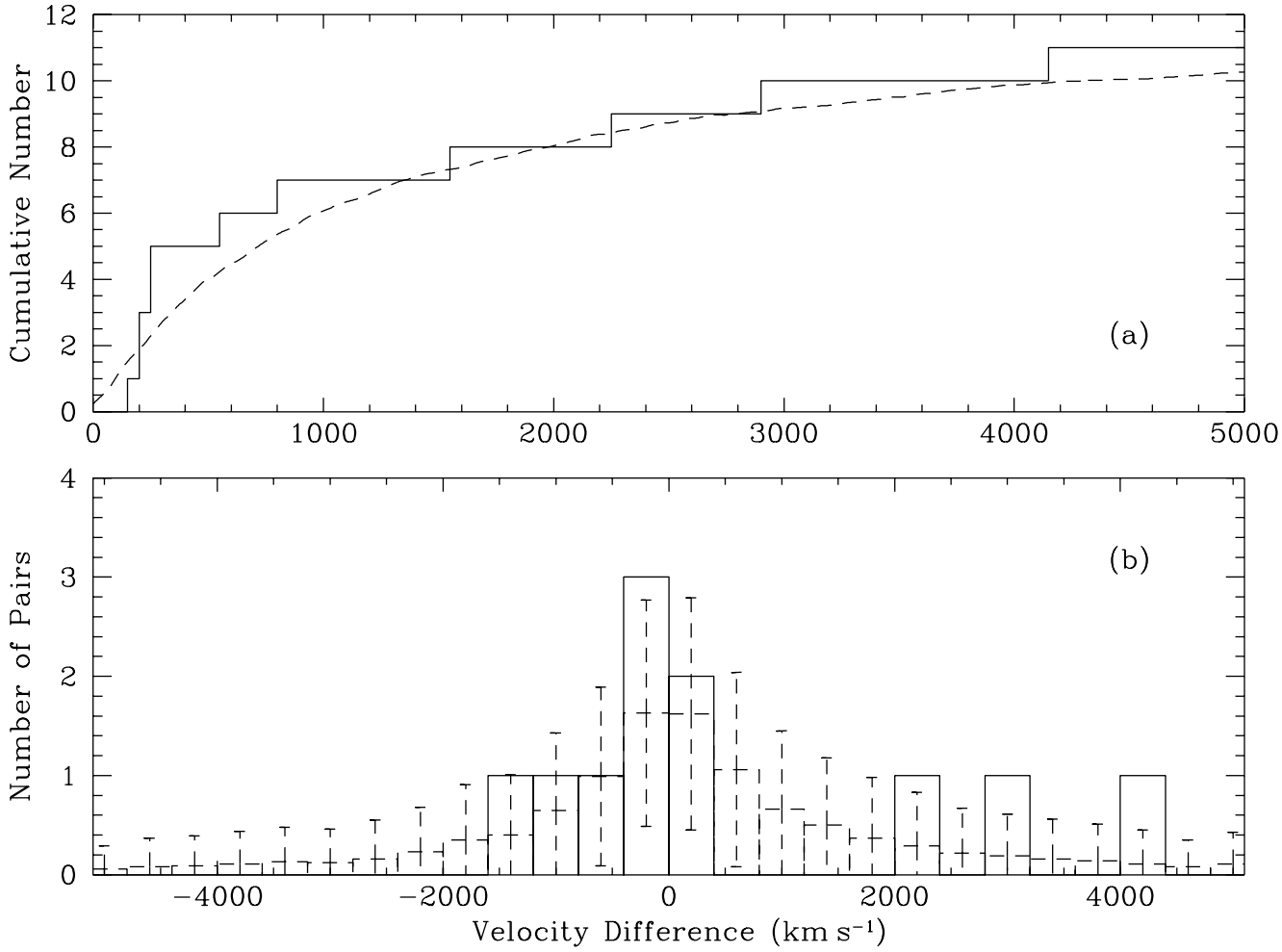

FIG. 4.—(*a*) Cumulative distribution (solid histogram) of velocity differences between each line in LB 9605 and its nearest neighbor in LB 9612. Dashed curve is the expected distribution for randomly-placed absorbers. (*b*) Distributions of observed (*solid line*) and random (*dashed line*) velocity differences in 400 km s^{-1} bins.

systems, with the result that we can only quote an upper limit on the size of absorbers. Alternatively, if we expand the velocity window in which we define a coincidence, we can more confident that we are counting all the common systems, but we are also more likely to include random coincidences. In fact, for $\Delta v = 1500$ km s^{-1} which corresponds to the velocity dispersions of some of the largest structures observed at $z < 2$ (e.g., rich clusters of galaxies; Zabludoff et al. 1993), we see six pairs and expect 7.3 ± 2.7, consistent with no real coincidences, and once again we obtain only an upper limit on the absorber size. From Figure 4*a*, the intermediate Δv that maximizes the number of coincident systems above the number of random coincidences is roughly 400 km s^{-1}.

The histograms of observed and expected velocity pairs in bins of $\Delta v = 400$ km s^{-1} are shown in Figure 4*b*. The distribution of velocity differences shows five pairs in the velocity range $-400 < \Delta v < 400$ km s^{-1}, and pairs at $\Delta v = -550$, -845, and -1586 km s^{-1}. We note one ambiguity in the assignment of a coincidence. Line 15 in LB 9612 could have been matched with either line 14 ($\Delta v = -220$ km s^{-1}) or 15 ($\Delta v = 260$ km s^{-1}) in LB 9605. The former match was selected because it has a smaller velocity separation; if we were to have paired the systems according to D94, such that their equivalent widths were more closely matched, then we would have called lines 15 in both quasars coincidences. In total, there are five possible coincidences between the two spectra within a velocity difference of $|\Delta v| < 400$ km s^{-1}, and 20 anticoincidences. The number of random coincidences expected in this velocity interval is $N_r = 3.2 \pm 1.8$. Therefore, the coincidences observed toward the paired LOSs to LB 9605 and LB 9612 are of marginal significance, $<2\ \sigma$, especially given the a posteriori selection of an optimum Δv matching window. Furthermore, the peculiar motions of the Lyα structures generated in hydrodynamical simulations have been found to be less than 150 kms^{-1} (Miralda-Escudé et al. 1996), so our use of 400 km s^{-1} likely overestimates the number of real coincidences.

In addition to the high probability of random coincidences, there are two uncertain line identifications that could affect the coincident count. Lines 14 and 15 in LB 9605 and line 8 in LB 9612 can be identified as members of C IV doublets at $z_{\rm abs} \simeq 0.9131$ and 1.1068, respectively. The redshift agreement between the components of the doublets is excellent ($\delta z < 0.0002$). Two of the lines have been identified as belonging to certain Lyα systems and were accordingly identified following the priorities of the Key Project identification procedure. If these are shown to be a C IV, then the number of coincidences drops to three, which is

consistent with the number of expected coincidences for randomly distributed absorbers.

The maximum significance we obtain for an excess number of common pairs above that expected for randomly placed absorbers is $\sim 2\,\sigma$. This implies that in most cases a single absorber is not intercepted by both LOS, and the absorbers are small compared to the LOS separation. Under this hypothesis, the equivalent widths of the coincident pairs should be uncorrelated (Charlton, Churchill, & Linder 1995). Figure 5 shows the correlation between the rest equivalent widths of the common systems in LB 9605 and LB 9612. Out of the five apparent coincidences, three have equivalent widths that agree with one another to within their respective errors. Using the observed equivalent width distribution of Lyα lines determined by the Key Project (Bahcall et al. 1993), we find that the probability of obtaining three pairs with equivalent widths lying within the quoted errors is not negligible $\sim 0.8\%$. However, recall the ambiguity in the pairing of the lines: although line 15 in LB 9612 was matched with line 14 in LB 9605, it equally well could have been matched with line 15 in LB 9605. In this latter case, we find there are four coincidences with similar equivalent widths, and the probability drops to 0.1%, indicating that the coincidences may not arise randomly.

For this reason, our attempt to establish an absorber size at these redshifts remains insecure, and we consider three possibilities: (1) all the coincidences are real, (2) two of the coincidences are real (after correcting the five observed coincidences for three random coincidences), and (3) none of the observed coincidences are real. We calculated the charcteristic radius using the maximum likelihood method outlined in D97, which is based on the counts of coincidences, N_C, and anticoincidences, N_A. In the following analysis, we assume the common Lyα lines arise in single coherent clouds and that the clouds are spherical and uniform in size. In this way, we may define the absorber radius R as the impact parameter that gave rises to lines with rest equivalent widths greater than our rest equivalent width detection limit. If however, the structures are small "cloudlets" that are spatially clustered, then our limits are more indicative of correlation lengths (discussed in more detail below). More data are required to establish with confidence which of these two models apply.

Figure 6 shows the likelihood distributions, $\mathscr{L}(R)$, as functions of absorber radius for the three cases considered above: (1) if we consider all of the coincidences to be real, i.e., $N_C = 5$ and $N_A = 20$, the most probable radius of the absorbers is 380 h^{-1} kpc. The cumulative probability distribution, also plotted in Figure 6 indicates a median radius of 410 h^{-1} kpc and 95% confidence lower and upper limits of $305 < R < 595\ h^{-1}$ kpc. (2) If we subtract the number of expected pairs ($N_r = 3$) from the total coincident count, such that $N_C = 2$, $N_A = 26$, we obtain a smaller characteristic radius of 275 h^{-1} kpc and median $R = 290\ h^{-1}$ kpc with 95% confidence limits of $240 < R < 390\ h^{-1}$ kpc. (3) Finally, if none of observed coincidences are real, then we derive a 95% confidence upper limit on the absorber radius of $R = 285\ h^{-1}$ kpc.

In the above analysis, we have not considered the effect of clustering on the estimated size of the absorbers. There is growing evidence for significant clustering of the absorbers, although there is as yet no consensus on the magnitude of the clustering. Fernández-Soto et al. (1996) has recently presented evidence for strong clustering of the absorbers based on observations of three quasars observed by Cowie et al. (1995). Using data from the High Resolution Echelle Spectrograph (HIRES) on the Keck 10 m telescope, Cowie et al. found that roughly half of the Lyα lines with $\log N$ (H I) > 14.5 have many weak associated C IV absorption systems. Fernández-Soto et al. used the redshifts of the C IV systems (because they are intrinsically narrower than the

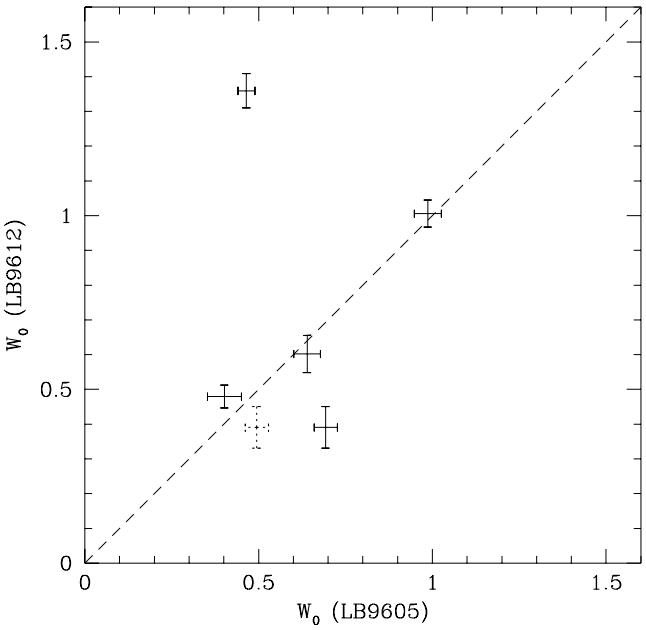

FIG. 5.—Correlation between the rest equivalent widths of the common lines in LB 9605 and LB 9612. Dotted error bars represent the alternate matching between lines 15 in Table 4 of both LB 9605 and LB 9612 (see text). Dashed line has unit slope.

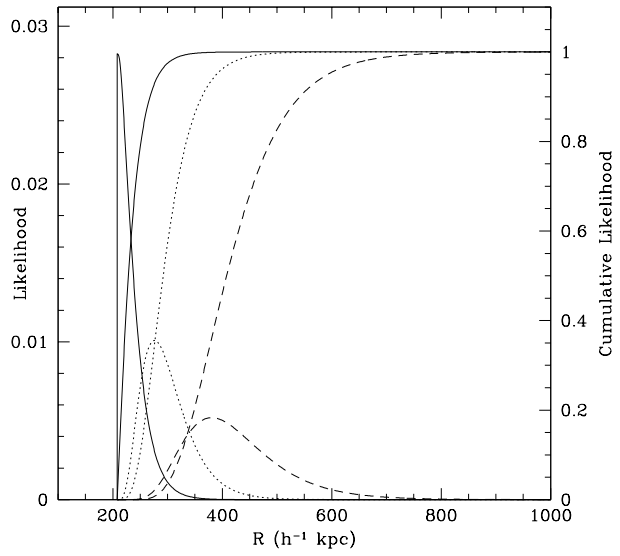

FIG. 6.—Likelihood distributions, $\mathscr{L}(R)$, normalized by their integrated likelihoods, as functions of absorber radius for three cases: (1) Five coincident and 20 anticoincident lines (*dotted curves*); the cumulative likelihood distribution (*monotonically increasing dotted line*) is also plotted from which lower and upper limits on the radius of the absorbers have been estimated. (2) Two coincidences and 26 anticoincidences (*dashed curves*). (3) None of the observed coincidences are real (*solid curves*).

Lyα lines and are therefore resolved) to calculate the two-point correlation function (ξ) of the Lyα absorbers at $z \sim 2.6$. Where associated C IV systems were not detected, the redshifts of the Lyα lines were used. Fernández-Soto et al. found $\xi \simeq 20$ on velocity scales of 200 km s^{-1}, consistent with the present-day galaxy-galaxy correlation function. This result is difficult to judge since it is still a matter of considerable debate whether the Lyα-only and metal-containing Lyα systems constitute the same population of objects, although a distinction between the two is becoming less meaningful (for a review, see Weymann 1995). For this reason, we have been careful to remove from our sample any Lyα absorption systems with associated metals.

The associated C IV absorption systems are a valid measure of the clustering amplitude of the Lyα absorbers if the C IV and Lyα systems probe the same absorbers. Although it is generally believed that the Lyα absorbers are somehow associated with galaxies, the degree and significance of this association is far from clear (Weymann 1995). Lanzetta et al. (1995) have shown that luminous galaxies nearly always give rise to Lyα absorption lines with rest equivalent widths $W_0 \gtrsim 0.3$ Å for impact parameters $\lesssim 160$ h^{-1} kpc. They also find a significant correlation between the strength of the line and impact parameter, which they use to argue that the Lyα absorption systems actually arise in the galaxies themselves. A reason for this apparent correlation may be that Lanzetta et al. include in their sample Lyα systems containing metals. If Lyα lines without corresponding metals are used, the correlation is marginal (Le Brun, Bergeron, & Boisse 1996). For this same reason, the absorber size that might be inferred from the Lanzetta et al. result (which one expects to be approximately less than or equal to their critical impact parameter if their interpretation is correct) may be somewhat smaller than those inferred from studies using adjacent LOS to background quasars (D95; Fang et al. 1996). Furthermore, recent studies by Le Brun et al. (1996) and Bowen, Blades, & Pettini (1996) find no evidence for a correlation between the strength of the Lyα line and impact parameter, weakening the argument for an intimate correlation between Lyα absorbers and galaxies. There are also a few examples of absorption systems arising in voids, far from the galaxy distribution, albeit their column densities are smaller than those in our sample (Morris et al. 1993; Stocke et al. 1995). Moreover, cosmological simulations at $z = 3$ by Haehnelt, Steinmetz, & Rauch (1996) show that clusters of narrow C IV absorption as observed by Cowie et al. (1995) can be produced when a LOS intersects protogalactic clumps embedded in an expanding large-scale filament. In the simulations, the multicomponent structure of the C IV absorption does not just occur when multiple clumps happen to be aligned with the LOS but also arises from complicated temperature and ionization structure inside the clumps.

The correlation amplitude measured by Fernández-Soto et al. (1996) is considerably larger than that determined by others. In a recent review paper, Cristiani (1995) derived the two-point correlation function using a large sample of Lyα lines with log (H I) > 13.8 from data with resolutions of between 9 and 14 km s^{-1}. He found only weak clustering on scales of 50–300 km s^{-1} (see also Chernomordik 1995; Cristiani et al. 1995). In the smallest velocity bin ($\Delta v = 100$ km s^{-1}), he found a highly significant (4.5 σ) signal in the two-point correlation function of $\xi \simeq 0.85 \pm 0.14$ for Lyα systems in the redshift range $1.7 < z < 3.1$. There is only one measure of the two-point correlation in a redshift range that overlaps the redshifts of the absorbers in our sample. Using the Key Project data, Ulmer (1996) found $\xi \simeq 1.8$ with significance (>90%) on scales of 250–500 km s^{-1} for absorbers in the redshift range $0 < z < 1.3$.

Because of the uncertainties in the amplitude of the correlations and the problems associated with evolving ξ to the redshift of our data, we only qualitatively consider the effect of clustering on the size of the absorbers. The redshift correlation functions determined by Fernández-Soto et al. (1996) and Cristiani (1996) do not allow one to directly infer the strength of the spatial clustering without knowledge of the structure and kinematics of the absorbers. However, we can estimate the expected number of coincidences for a clustered distribution if we assume their redshift correlation functions roughly predict the probability of obtaining a coincidence in adjacent LOSs. According to the definition of the correlation function, the probability of finding a line within a redshift difference of Δz of another is given by

$$dP = n_z(1 + \xi)\Delta z ,$$

where n_z is the number density of systems. Recall, that for randomly distributed absorbers ($\xi = 0$), the expected number of coincidences was 3.2 ± 1.8, as shown in Figure 4*b*. For weak correlations (i.e., $\xi \simeq 1$), the expected number of coincidences is twice this number, consistent with the observed number of coincidences. Thus, weak clustering is not inconsistent with case (3) (see above) that implies an upper limit on size of the absorbers, and in fact reinforces this interpretation. On the other hand, for strong clustering such as that implied by Fernández-Soto et al.'s result, we expect that *most, if not all*, of the Lyα lines in our sample would be coincidences. In fact, we found only *one* coincidence within a velocity difference of 200 km s^{-1}, the scale over which significant clustering was detected, and *none* within 150 km s^{-1}, where the correlation amplitude is strongest.

Differences in equivalent widths and relative velocities of the common systems provide information about the homogeneity and internal kinematics of the absorbers since the quasar LOS pierce the Lyα absorbers at different locations. From studies of gravitationally lensed quasars with characteristic pathlength separations at the redshift of the absorbers of a few kpc, the absorbers are homogeneous and their internal motions are small, less than 10–20 km s^{-1} (Smette et al. 1992, 1995; Bechtold & Yee 1995). In D94, we presented evidence for significant inhomogeneities in the absorbers, as well as a marginally significant rms velocity difference of 65 km s^{-1} from observations of the physical pair Q1343+2640A, B with separation $\sim 40h^{-1}$ kpc. From the common lines of Q0107−025A, B, we found a statistically significant velocity difference of ~ 100 km s^{-1} over scales of several hundred kpc, implying that the absorbers are still remarkably quiescent on these scales. The rms velocity difference, $\Delta v_{\rm rms} \simeq 260$ km s^{-1}, of the five apparently coincident lines in the spectra of LB 9605 and LB 9612 also exceeds the typical velocity error, but interpretation of this result is hampered by our uncertainty over how many, if any, of the coincidences are real. As shown in Figure 5, if the coincidences are indeed real, the absorbers must have remarkably smooth column density distributions on scales of several hundred kpc, in contrast to the results of previous studies of widely separated quasar pairs.

Although we favor the interpretation that none of the coincidences are real (case 3) which gives an upper limit on the absorber radius of $285h^{-1}$ kpc, we cannot rule out larger clouds that are remarkably smooth on scales of the LOS separation of the quasar pair. Nor can we reject a model involving a distribution of absorber sizes. The high level of correlation in the equivalent widths for the observed coincidences, which make up $\lesssim 20\%$ of the total sample, could be explained if there is a rare population of large, homogeneous absorbers in addition to a population of small absorbers which dominates the counts (but see § 5). We are reluctant to introduce any more parameters into the analysis at this time given the limited data sample.

5. SUMMARY AND DISCUSSION

Recent ground-based observations of the high-redshift quasar pair Q1343+2640 A ($z_{em} = 2.029$) and Q1343+2640 B ($z_{em} = 2.031$), interpreted in terms of the same simple model assumed above (i.e., identical, spherical absorbers) suggest a characteristic radius of the absorbers of 125 h^{-1} kpc and median $R = 185h^{-1}$ kpc, with 95% lower and upper bounds of $80 < R < 610\ h^{-1}$ kpc at $z \simeq 2$ (D94; see also Bechtold et al. 1994 and Fang et al. 1996). Observations of a lower redshift pair Q0107−025A ($z_{em} = 0.956$) and Q0107−025 B ($z_{em} = 0.952$) in the redshift range $0.48 \leq z \leq 0.89$, imply lower limits on the transverse radius of the absorbers of 140 h^{-1} to 160 h^{-1} kpc. Maximum likelihood estimates of the characteristic radii for spherical clouds, give a most probable radius of 505 h^{-1} kpc and median $R = 645\ h^{-1}$ kpc, with 95% confidence that the characteristic radius lies in the range $345 < R < 1520\ h^{-1}$ kpc. (The radii quoted here are different from those given in D94 and D95 because of an error in our derivation of the likelihood distribution [see D97 for details].)

We note that the characteristic radius estimated from the data of Q1343+2640A, B was obtained using 5 σ Lyα lines with no rest equivalent width detection limit imposed. In contrast, in this paper and in our analysis of the data of Q0107−025A, B, we considered only the region of the spectrum where 5 σ lines with $W_0 > 0.32$ Å would be detected. In order to compare the absorber radius inferred from Q1343+2640A, B with that of Q0107−025A, B and the results presented in this paper, we must make the samples uniform. If we impose the same detection criteria on the Q1343+2640A, B data, then we must discard all lines in Table 1 of D94 with $\lambda < 3525$ Å and $W_0 \leq 0.32$ Å. This has the effect of cutting the number of lines in the new sample by more than a factor of two. The new sample contains 2 coincidences and 4 anticoincidences, from which we derive a most probable radius of 50 h^{-1} kpc, with 95% confidence limits of $30 < R < 230\ h^{-1}$ kpc. Bechtold et al. (1994) have also looked at this pair. Imposing the same detection criteria on their linelist (Crotts et al. 1994; Table 1) and discarding the spectrum shortward of $\lambda = 3500$ Å, three coincidences and two anticoincidences remain. The radius implied by this sample is 100 h^{-1} kpc, with 95% lower and upper bounds of $60 < R < 2620\ h^{-1}$ kpc. The differences in the number of coincidences and anticoincidences is *entirely* due to the different spectral resolutions of the data. One of the coincidences in the Bechtold et al. (1994) data appears to be a blend of two coincidences in our higher resolution data, with one of the lines in each pair falling below the equivalent width limit (cf. line pair A9-B16 in Crotts et al. 1994 and pairs A7-B4 and A8-B5 in D94). This discussion serves to highlight some of the pitfalls of this kind of analysis, particularly when dealing with such small numbers of lines.

Figure 7 shows the estimated radius of the Lyα absorbers in three redshift regimes, where the value of the radius estimated by D94 for the pair Q1343+2640A, B has been plotted since it is consistent with the radii derived above, but has smaller error bars. These observations span a large redshift range $0.5 \lesssim z \lesssim 2.1$, corresponding to roughly a third of the age of the universe, and imply a growth in the radius of the Lyα absorbers of a factor of 3–4 from $z \simeq 2$ to $z \simeq 0.7$. There are two other estimates of the absorber radius at $z \sim 2$ published in Fang et al. (1996). However, it may be misleading to plot these estimates in Figure 7 because those radii were calculated assuming a cutoff rest equivalent width of $W_0 > 0.40$ Å (compared to the value $W_0 > 0.32$ Å used in this paper), and there is evidence for a correlation of absorber radius with column density, with the high column density clouds being larger in extent than the low column density clouds (D97). For q_0, the apparent evolution in absorber radius is less pronounced.

As discussed in the previous section, we cannot yet distinguish between coherent versus correlated structures, although for simplicity we have assumed the former in our analysis of the size of the absorbers. It is also possible that the coincidences observed in D94, D95 and this paper arise as a result of clustering of the absorbers, such that the apparent evolution we observe in Figure 7 actually represents an increase in the correlation length of the clustering, rather than a growth in the physical size of the absorbers with cosmic time. The issue of whether the parameter we are measuring is the physical radius of a coherent cloud or the correlation length of clustered absorbers will require substantially more data to resolve.

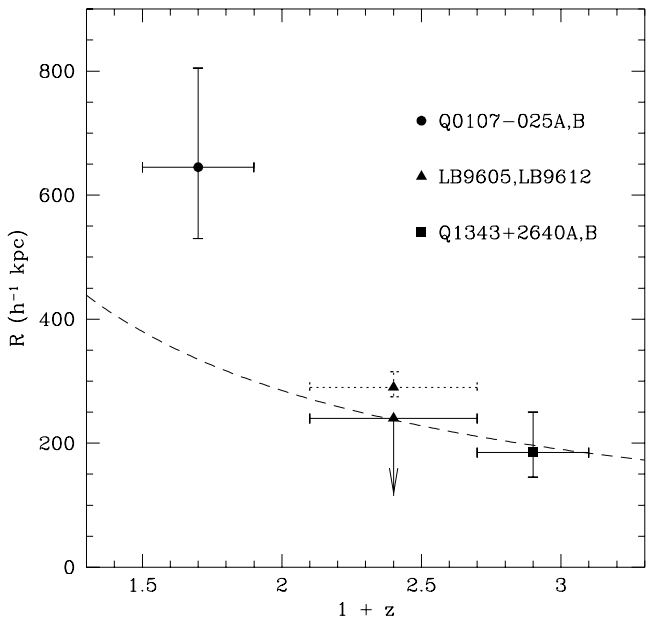

FIG. 7.—Estimates of the median radius of Lyα absorbers in three redshift intervals, indicated by the horizontal error bars. Vertical error bars represent 68% confidence limits. Vertical dotted error bars give the limits on the absorber radius for two coincidences and 26 anticoincidences (i.e., having corrected the five observed coincidences for three random coincidences [see § 4]). The dashed line represents the radius evolution for a freely expanding Hubble sphere with arbitrary normalization.

Charlton et al. (1995) and D97 have presented methods of distinguishing between correlated versus coherent structures by analysing the correlation (or lack of correlation) in the equivalent widths of the common systems.

An alternative interpretation for the trend in Figure 7 is given in Fang et al. (1996). They note that the characteristic radii inferred from quasar pairs depend on the LOS separations, in the sense that pairs with larger proper separation give larger absorber radii. This can be explained if there is a distribution of absorber sizes, or the absorbers are clustered. In the first case, a population of small clouds will produce a higher incidence of anticoincidences for both closely separated pairs as well as widely separated pairs resulting in a smaller inferred radius. However, as long as there is a population of large clouds with transverse size greater than the LOS separation, the lower limit of the cloud size cannot be less than the transverse separation of the pair. Therefore, estimates based on observations of widely separated pairs will be biased toward larger absorber radii. A similar bias holds for absorbers that are correlated over a range of scales.

In Figure 8, we have reproduced Fang et al.'s Figure 5 which shows the apparent trend in inferred absorber radius with pair separation. The radii were estimated for six pairs with angular separations ranging from $\sim 10''$ to $3'$. In order to obtain a uniform sample only those lines with rest equivalent widths $W_0 > 0.40$ Å were used. Coincidences were defined within a velocity differences of $\Delta v < 150$ km s^{-1}. In the sample of Lyα lines for LB 9605, LB 9612, there are *no* coincidences within this velocity difference, implying an upper limit on the inferred radius for redshifts $1.06 < z < 1.69$. With the addition of this new point in Figure 8, the trend of radius versus separation is less significant. The upper limit derived in this paper argues *against* there being a population of large clouds at high redshift, in an apparent contradiction with the estimates based on the high-redshift quasar group Q1623+2651A, B and Q1623+2653, reported in Fang et al. More data of this group and other high-redshift widely-separated pairs are required to settle this.

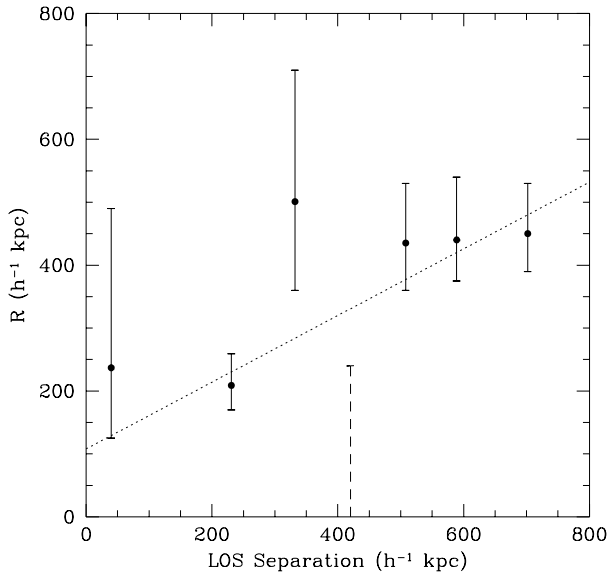

FIG. 8.—Inferred median radius as a function of pair separation reproduced from Fang et al. (1996; Fig. 5). The dotted line indicates Fang et al.'s least-squares fit to the six quasar pairs considered in their paper. The 1 σ upper limit derived in this paper from the LB 9605, LB 9612 pair is indicated by the dashed error bar.

Recent hydrodynamical simulations exhibiting hierarchical clustering are able to reproduce the essential properties (e.g., distributions of column density and Doppler parameter) of the Lyα forest. In these simulations, the low column-density absorption systems arise in sheetlike or filamentary structures with coherence lengths consistent with those estimated from quasar pairs (Cen et al. 1994; Hernquist et al. 1996; Miralda-Escudé et al. 1996). To date, the simulations have not been evolved below $z = 2$, so it is difficult to interpret the apparent evolutionary growth of the Lyα absorbers in terms of those models. However, since gravity has the effect of amplifying initial anisotropies, the correlation or coherence lengths of these anisotropies may be expected to grow in size as gravitational clustering evolves (Pauls & Melott 1995). Moreover, the simulations show that many of the low column-density Lyα lines, produced in regions of low overdensity ($\rho/\bar{\rho} \sim 1$–10), are not in dynamical equilibrium and are still expanding with residual Hubble flow (Hernquist et al. 1996). Pancake-like structures are expected to be expanding about 30% faster than the Hubble flow (Haehnelt 1996). Superimposed on Figure 7 is the expected evolution of the absorber radius for a freely expanding Hubble sphere, $R \propto (1 + z)^{-1}$. The observed evolution in absorber radius is well-represented by free Hubble expansion at redshifts $z < 2$, although better limits are needed in order to constrain the evolutionary character of the Lyα absorber size.

Some of the growth in absorber radius may also be related to the decline in the UV background. The space density of quasars and the star formation rates peak at redshifts $z > 2$, and fall off at lower redshifts. Impey et al. (1996) have suggested that the transition in the absorber number density evolution (from rapid evolution at $z \gtrsim 2$ to a flattening of dN/dz at low redshifts) could be related to the drop in the background UV flux causing the absorbers to become more neutral. Thus, a fixed column density (corresponding to the rest equivalent width detection limit) would be measured at a larger impact parameter. The apparent increase in the radius therefore does not necessarily correspond to a physical growth but may result from an increase in the neutral hydrogen fraction of the absorbers. The combination of a net increase in the size of the absorbers with a change in the ionization level may explain the leveling off of the number density of Lyα systems at low redshift.

In summary, we have presented FOS G270H spectra of the quasar pair, LB 9605 and LB 9612 in order to measure the size of the Lyα absorbers. The quasars are separated by $1\farcm65$ corresponding to a linear separation of 412 h^{-1} kpc at $z = 1.83$. We detected five coincident absorption lines within a velocity difference of 400 km s^{-1} in the redshift range $1.05 < z < 1.69$, and 20 anticoincidences. The significance of the observed coincidences is less than 2 σ. On this basis, we argued that none of the observed coincidences are likely to be real, and we placed an upper limit on the absorber radius of 285 h^{-1} kpc assuming spherical absorbers. Together with estimates at $z \simeq 0.7$ and $z \simeq 2.1$, this suggests evolutionary growth in the radius of the Lyα absorbers with cosmic time. However, we could not exclude the possibility that all the observed coincidences are real, from which we obtained a characteristic radius of 380 h^{-1}

kpc with 95% confidence that it lies in the range $305 < R < 595\ h^{-1}$ kpc. Observations of more pairs, particularly at redshifts $z > 2$, will be required to confirm the apparent evolution in absorber radius presented here. The analysis will be difficult due to the problems of blending and metal-line contamination, and will likely require the development of new statistical techniques.

This research was supported by NASA grant GO5320.01-93A from the Space Telescope Science Institute, AURA Inc., and NSF grant AST 93-20715. We thank Adrian Melott, Buell Jannuzi, Jordi Miralda-Escudé, and Neal Katz for useful discussions. We are grateful to Tom Aldcroft for allowing us to use his spectral analysis software.

REFERENCES

Aldcroft, T. 1993, Ph.D. thesis, Stanford Univ.
Bahcall, J. N., et al. 1993, ApJS, 87, 1
Bahcall, J. N., et al. 1996, ApJ, 457, 19
Bechtold, J., Crotts, A. P. S., Duncan, R. C., & Fang, Y. 1994, ApJ, 437, L83
Bechtold, J., & Yee, H. K. C. 1995, AJ, 110, 1984
Bowen, D. V., Blades, J. C., & Pettini, M. 1996, ApJ, 464, 141
Cen, R., Miralda-Escudé, J., Ostriker, J. P., & Rauch, M. 1994, ApJ, 437, L9
Charlton, J. C., Churchill, C. W., & Linder, S. M. 1995, ApJ, 452, L81
Chernomordik, V. V. 1995, ApJ, 440, 431
Cowie, L. L., Songaila, A., Kim, T.-S., & Hu, E. M. 1995, AJ, 109, 1522
Cristiani, S. 1996, in Proc. Internet. School of Phys. "Enrico Fermi," Dark Matter in the Universe, ed. S. Bonometto, J. R. Primack, & A. Provenzal (Amsterdam: IOS), 137
Cristiani, S., D'Odorico, S., Fontana, A., Giallongo, E., & Savaglio, S. 1995, MNRAS, 273, 1016
Crotts, A. P. S., Bechtold, J., Fang, Y., & Duncan, R. C. 1994, ApJ, 437, L79
Dinshaw, N., Foltz, C. B., Impey, C. D., Weymann, R. J., & Morris, S. L. 1995, Nature, 373, 223 (D95)
Dinshaw, N., Impey, C. D., Foltz, C. B., Weymann, R. J., & Chaffee, F. H. 1994, ApJ, 437, L87 (D94)
Dinshaw, N., Weymann, R. J., Impey, C. D., Foltz, C. B., Morris, S. L., & Ake, T. 1997, ApJ, 491, 45 (D97)
Elowitz, R. M., Green, R. F., & Impey, C. D. 1995, ApJ, 440, 458 (E95)
Fang, Y., Duncan, R. C., Crotts, A. P. S., & Bechtold, J. 1996, ApJ, 462, 77
Fernández-Soto, A., Lanzetta, K. M., Barcons, X., Carswell, R. F., Webb, J. K., & Yahil, A. 1996, ApJ, 460, L85
Haehnelt, M. G. 1996, in Cold Gas at High Redshift, ed. M. N. Bremer et al. (Dordrecht: Kluwer), 109
Haehnelt, M. G., Steinmetz, M., & Ruch, M. 1996, ApJ, 465, L95
Hernquist, L., Katz, N., Weinberg, D. H., & Miralda-Escudé, J. 1996, ApJ, 457, L51
Impey, C. D., Petry, C. E., Malkan, M. A., & Webb, W. 1996, ApJ, 463, 473
Lanzett, K. M., Bowen, D. V., Tytler, D., & Webb, J. K. 195, ApJ, 442, 538
Le Brun, V., Bergeron, J., & Boisse, P. 1996, A&A, 306, 691
Lindler, D., Bohlin, R., Hartig, G., & Keyes, C. 1993, FOS Instrum. Sci. Rep. CAL/FOS-088 (Greenbelt, MD: STScI)
Miralda-Escudé, J., Cen, R., Ostriker, J. P., & Rauch, M. 1996, ApJ, 471, 582
Morris, S. L., Weymann, R. J., Dressler, A., McCarthy, P. J., Smith, B. A., Terrile, R. J., Giovanelli, R., & Irwin, M. 1993, ApJ, 419, 524
Morton, D. C., York, D. G., & Jenkins, E. B. 1988, ApJS, 68, 449
Pauls, J. L., & Melott, A. L. 1995, MNRAS, 274, 99
Schneider, D. P., et al. 1993, ApJS, 87, 45
Smette, A., Robertson, J. G., Shaver, P. A., Reimers, D., Wisotzki, L., & Kóhler, T. 1995, A&AS, 113, 199
Smette, A., Surdej, J., Shaver, P. A., Foltz, C. B., Chaffee, F. H., Weymann, R. J., Williams, R. E., & Magain, P. 1992, ApJ, 389, 39
Stocke, J. T., Shull, J. M., Penton, S., Donahue, M., & Carilli, C. 1995, ApJ, 451, 24
Tytler, D., Fan, X.-M., Burles, S., Cottrell, L., Davis, C., Kirkman, D., & Zuo, L. 1995, in Proc. ESO Workshop on QSO Absorption Lines, ed. G. Meylan (Heidelberg: Springer), 289
Ulmer, A. 1996, ApJ, 473, 110
Weymann, R. J. 1995, in Proc. ESO Workshop on QSO Absorption Lines, ed. G. Meylan (Heidelberg: Springer), 3
Zabludoff, A. I., Geller, M. J., Huchra, J. P., & Vogeley, M. S. 1993, AJ, 106, 1273
Zhang, Y., Anninos, P., & Norman, M. L. 1995, ApJ, 453, L57